



# Synthesis and Properties of the $\text{LiMn}_2\text{O}_4$ Cathode Material for Lithium-ion Batteries

Qian Yu <sup>a\*</sup>, Pinjiang Li <sup>a</sup> and Qian Guo <sup>a</sup>

<sup>a</sup> North China University of Water Resources and Electric Power, Zhengzhou, Henan, China.

## Authors' contributions

This work was carried out in collaboration among all authors. All authors read and approved the final manuscript.

## Article Information

DOI: 10.9734/IRJPAC/2024/v25i3852

## Open Peer Review History:

This journal follows the Advanced Open Peer Review policy. Identity of the Reviewers, Editor(s) and additional Reviewers, peer review comments, different versions of the manuscript, comments of the editors, etc are available here: <https://www.sdiarticle5.com/review-history/115430>

Received: 02/02/2024

Accepted: 06/04/2024

Published: 12/04/2024

Short Research Article

## ABSTRACT

Spinel  $\text{LiMn}_2\text{O}_4$  was synthesized by high-temperature solid-state method with lithium salt and manganese salt as raw materials, which were mixing with anhydrous ethanol as solvent under stirring, and calcining at high temperature in the oxygen atmosphere. X-ray diffraction (XRD) and scanning electron microscope (SEM) showed that the size of lithium manganese particles with spinel structure was 80 to 200 nm, and the particle size distribution was uniform. The results showed that the prepared  $\text{LiMn}_2\text{O}_4$  sample sintered at 700°C exhibited superior electrochemical performance when used as a cathode material for lithium-ion batteries with a voltage window of 2.5–4.8 V. The first charge-discharge specific capacity and first discharge capacity can reach 158.0  $\text{mAh}\cdot\text{g}^{-1}$  and 138.4  $\text{mAh}\cdot\text{g}^{-1}$ , respectively, at 0.1  $\text{A}\cdot\text{g}^{-1}$  current density, and the first Coulomb retention efficiency is 87.6%. The discharge specific capacity of the  $\text{LiMn}_2\text{O}_4$  material can be maintained at 114  $\text{mAh}\cdot\text{g}^{-1}$  when the test current density was returned to 0.1  $\text{A}\cdot\text{g}^{-1}$  after 60 cycles.

**Keywords:** High-temperature solid-phase method; lithium manganese; lithium-ion battery; electrochemical performance.

\*Corresponding author: E-mail: yxn0125@foxmail.com;

## 1. INTRODUCTION

“Nowadays, lithium-ion batteries (LIBs) are playing an increasingly important role in electrochemical energy storage devices” [1-4]. “Therefore, improving the energy density of LIBs is required for high performance electric vehicles in terms of their driving distance. At present, high specific energy is the continuous pursuit of batteries because the low specific capacity of cathode materials is an important factor limiting the energy density of LIBs. Therefore, a lot of research work is devoted to exploring cathode materials with a higher energy density” [5,6].

LiMn<sub>2</sub>O<sub>4</sub> is one of the promising candidate as the new generation of lithium-ion battery cathode material [7] due to abundant resources, low cost, friendliness to environment, high chemical potential and safety [8-10]. Moreover, because of its unique three-dimensional tunneling structure, it is more favorable to the embedding and detachment of Li<sup>+</sup>, which benefit to higher power and energy density [11-14]. However, the cycling performance of LiMn<sub>2</sub>O<sub>4</sub> is still limited by some problems such as Jahn-Teller deformation and Mn dissolution [15,16]. Therefore, so many approaches have been investigated to enhance the spinel-type cathode materials by doping techniques. Some metal ions like Al, Mg, Zn, Co or Ni were doping to improve electrical conductivity, stability, cycle life, and performance in extreme conditions, such as high temperatures and high-current charging/discharging [17-21].

In this study, pure LiMn<sub>2</sub>O<sub>4</sub> was prepared by high-temperature solid-state method. The microstructure and crystal structure of the material were observed by X-ray diffraction and scanning electron microscopy, and the electrochemical properties of the material were tested by constant current charge and discharge, cyclic voltammetry and AC impedance. The results indicate that the prepared LiMn<sub>2</sub>O<sub>4</sub> via the high-temperature solid-phase approach displays improved cycling capacity and capacity retention, highlighting its enhanced electrochemical properties.

## 2. METHODOLOGY

### 2.1 Material Preparation

LiMn<sub>2</sub>O<sub>4</sub> was synthesized by a solid-state reaction at high temperature in air with Li<sub>2</sub>CO<sub>3</sub> and MnCO<sub>3</sub> as raw materials. To compensate for losses during calcination, Li excess of 0.05 mol.

Analytical grade chemicals Li<sub>2</sub>CO<sub>3</sub> and MnCO<sub>3</sub> in stoichiometric amounts were dissolved in anhydrous ethanol. The mixture was stirred about 30 minutes at 60 °C and dried in a vacuum at 100 °C for 6 h. The mixed powder was calcined in a 700 °C muffle furnace at a heating rate of 5 °C·min<sup>-1</sup> for 12 hours under oxygen conditions, and then cooled to room temperature to obtain the target sample.

### 2.2 Materials Characterization

The crystal structures of the samples were identified by powder X-ray diffraction performed using a D8 Advanced X-ray diffraction (XRD, Bruker, Cu K $\alpha$  radiation, Germany) from 10° to 90°. The surface morphologies of the sample were observed with a Nova nano SEM450 field emission scanning electron microscopy (FEI, USA).

### 2.3 Electrochemical Measurements

The electrode material was prepared with a weight ratio of 80% active material, 10% acetylene black, and 10% binder (polyvinylidene fluoride, PVDF, dissolved in N-methyl-2-pyrrolidone, NMP, in a certain volume), and then coated on aluminum foil to obtain a positive electrode plate, which was dried under vacuum at 90°C for 12 hours. A CR2032 button cell was assembled using a Li plate as the negative electrode, a Celgard2400 polypropylene microporous membrane, and an electrolyte of 1.0 mol/L LiPF<sub>6</sub> in EC: DMC: EMC=1:1:1 Vol% with 1.0% VC solution in an argon glove box.

The constant current charge and discharge mode was achieved with a multichannel battery tester (Shenzhen Neware, BTS, P. R. China). Cyclic voltammetry (CV) and impedance test were operated between 2.5 and 4.8 V with Autolab AUT86647 Electrochemical AC Impedance Comprehensive Tester.

## 3. RESULTS AND DISCUSSION

### 3.1 Physical Phase Analysis

In order to understand the elemental composition transformations occurring in the different annealing temperatures, as-synthesized LiMn<sub>2</sub>O<sub>4</sub> samples were characterized using XRD (Fig. 1). All the XRD patterns match very well with the XRD pattern for phase pure LiMn<sub>2</sub>O<sub>4</sub> (PDF #35-0782). Hence, successful preparation of LiMn<sub>2</sub>O<sub>4</sub>

through experimental techniques is achieved. Notably, the sample at 600 °C displays a weaker intensity in its characteristic peak. Additionally, with increasing temperature, the characteristic peaks of the sample become sharper, and the full width at half maximum (FWHM) of the peak reduces. The high crystallinity and large grain size of the sample can be attributed to the high calcination temperature, facilitating full reactions of the reactants. In a spinel structure, the ratio  $R=(I_{(311)}/I_{(400)})$  of diffraction peak intensities from the (311) and (400) crystal faces reflects the degree of spinel lattice distortion [22]. A smaller  $R$  indicates sharper lattice distortion and a more complete crystal structure.

For  $\text{LiMn}_2\text{O}_4$  samples,  $R$  values at calcination temperatures of 600 °C, 700 °C and 800 °C were found to be 0.992, 0.9517 and 0.9687, respectively. Notably, the sample calcined at 700 °C exhibited the smallest  $R$  value, indicating the least lattice distortion and a more orderable internal structure. This suggests that the potential for better electrochemical performance compared to samples calcined at 800 °C and 600 °C.

### 3.2 Morphological Analysis

Fig. 2 illustrates that lithium manganate with a spinel structure displays an irregular polyhedral shape, a distinct layered structure, and individual particle sizes ranging from 80-200 nm, with some minor agglomeration. This agglomeration may occur during the high-temperature sintering process in solid-phase preparation. The sample shows more pronounced and uneven agglomeration at 600 °C. However, particles at 700 °C exhibit uniform sizes, smooth edges, excellent crystallinity, and high phase purity. Notably, at 800 °C, the particle sizes vary, and some agglomeration is observed.

### 3.3 Electrochemical Performance Analysis

In order to test the electrochemical performance of  $\text{LiMn}_2\text{O}_4$  as cathode material for lithium ion batteries, Fig. 3 shows the cv curve of  $\text{LiMn}_2\text{O}_4$  samples with calcination temperature of 700 °C using cyclic voltammetry.

Cyclic voltammetry was utilized to assess the electrochemical properties of  $\text{LiMn}_2\text{O}_4$  as a cathode material for lithium-ion batteries. The results, displayed in Fig. 3, showcase the CV curves of  $\text{LiMn}_2\text{O}_4$  electrodes tested at scanning rates ranging from 0.2 to 1.0  $\text{mV s}^{-1}$  and voltages

from 2.5 to 4.8 V. The curves illustrate a noticeable reduction peak about 2.7 V, indicating the reduction of lithium manganate  $\text{Mn}^{4+}$  to  $\text{Mn}^{3+}$ . Additionally, an oxidation peak at 3.0 V signifies the electrochemical oxidation of  $\text{Mn}^{3+}$  to  $\text{Mn}^{4+}$ . Redox peaks at 4.0 V and 4.2 V correspond to lithium extraction and insertion, respectively. An additional weak oxidation peak at 4.8 V is attributed to the high voltage levels. The consistent shape of the redox curves and smaller peak potential difference indicate better reversibility performance, suggesting minimal capacity loss and enhanced cycling stability of the material.

To explore the electrochemical performance of the synthesized  $\text{LiMn}_2\text{O}_4$  material, tests were conducted to assess its multiplicity and cycling performance.

Fig. 4 displays the charge/discharge performance curves of  $\text{LiMn}_2\text{O}_4$  half-cells within a test voltage window from 2.5 V to 4.8 V. The  $\text{LiMn}_2\text{O}_4$  samples were tested at different currents: 0.1  $\text{A g}^{-1}$ , 0.2  $\text{A g}^{-1}$ , 0.5  $\text{A g}^{-1}$ , 1  $\text{A g}^{-1}$ , 2  $\text{A g}^{-1}$ , and 5  $\text{A g}^{-1}$ .

From the figure, it is evident that the sample electrode calcined at 700 °C exhibited the highest charge/discharge capacity among the three samples. It displayed a first charging capacity of 158.0  $\text{mAh g}^{-1}$ , a first discharge capacity of 138.4  $\text{mAh g}^{-1}$ , and a first Coulomb retention efficiency of 87.6%. When the test current was reverted to 0.1  $\text{A g}^{-1}$ , the discharge specific capacity of this  $\text{LiMn}_2\text{O}_4$  material remained stable at 114  $\text{mAh g}^{-1}$ .

For the sample electrodes calcined at 800 °C, the first charge/discharge specific capacities reached 128.75  $\text{mAh g}^{-1}$  and 104.92  $\text{mAh g}^{-1}$ , respectively, while the final capacities were 110.99  $\text{mAh g}^{-1}$  and 86.89  $\text{mAh g}^{-1}$ , respectively.

Fig. 5 displays the first three charge-discharge curves of the  $\text{LiMn}_2\text{O}_4$  electrode sample with a calcination temperature of 700 °C. The measurements were taken at a constant current density of 0.1  $\text{A g}^{-1}$ . The first three-turn discharge curve exhibits two distinct discharge plateaus at approximately 4.0 V and 2.7 V. Conversely, the first three-turn charging curve displays two clear charging plateaus at around 3.0 V and 4.1 V. The voltage levels of the charging and discharging plateaus align with the redox peaks observed on the CV curves, which represent the electrochemical oxidation and reduction reactions of  $\text{LiMn}_2\text{O}_4$ , respectively.

Fig. 6 displays the cycling performance of the  $\text{LiMn}_2\text{O}_4$  electrode. At a current density of  $0.1 \text{ A g}^{-1}$ , the charge/discharge specific capacities of  $\text{LiMn}_2\text{O}_4$  were initially  $148.27 \text{ mAh g}^{-1}$  and  $133.35 \text{ mAh g}^{-1}$ . After 100 cycles, the charge/discharge capacities ranged between  $98.42 \text{ mAh g}^{-1}$  and  $97.85 \text{ mAh g}^{-1}$ .

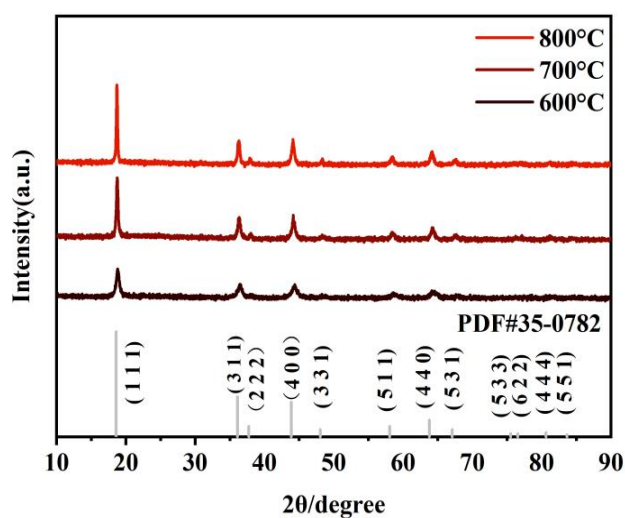


Fig. 1. XRD patterns of as-synthesized  $\text{LiMn}_2\text{O}_4$  samples at different annealing temperatures

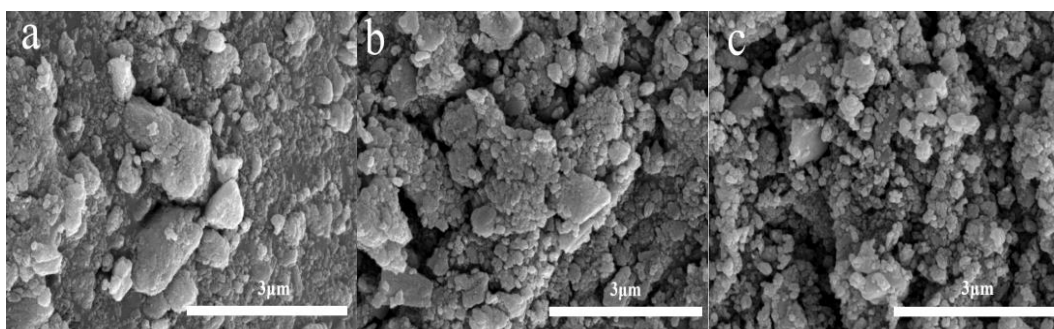


Fig. 2. SEM images of  $\text{LiMn}_2\text{O}_4$  samples with calcination temperatures of 600, 700, and 800 °C

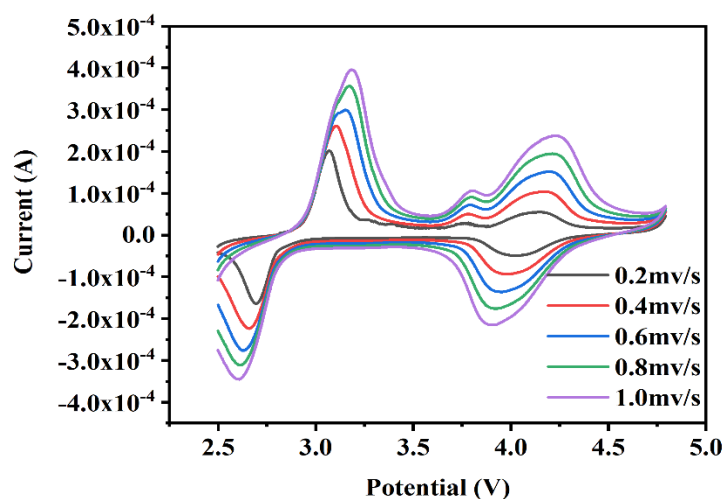


Fig. 3. CV graph of  $\text{LiMn}_2\text{O}_4$  sample with a calcination temperature of 700 °C

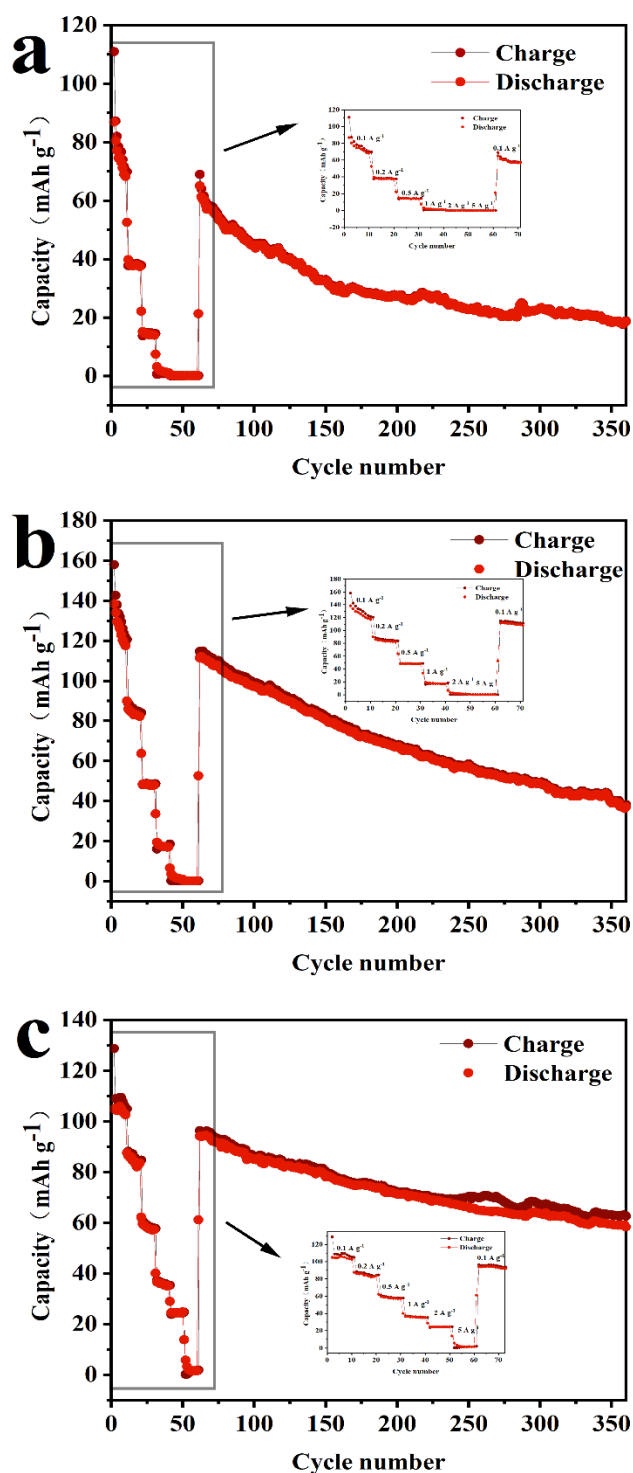


Fig. 4. The charging and discharging capabilities of LiMn<sub>2</sub>O<sub>4</sub> samples at calcination temperatures of 600 °C, 700 °C and 800 °C

Fig. 7 illustrates the comparison of the AC impedance of the LiMn<sub>2</sub>O<sub>4</sub> electrode before and after cycling. The Nyquist diagrams display two components: a semicircle in the high-

frequency region and a diagonal line in the low-frequency region. The semicircle represents the charge transfer resistance ( $R_{ct}$ ), while the diagonal line corresponds to the Warburg

impedance ( $Z_w$ ) related to  $\text{Li}^+$  diffusion within the material [23,24]. The AC impedance ( $Z$ ) is composed of a real part ( $Z'$ ) and an imaginary part ( $Z''$ ). A smaller semicircle radius indicates lower charge transfer resistance, while a steeper diagonal line slope suggests reduced lithium ion diffusion resistance [25,26].

Comparing the curves before and after cycling, there are similar semicircular arcs with slightly larger slope in the post-cycle curve, indicating decreased ion diffusion impedance in the half-cell after cycling. In this context,  $R_s$  in the circuit diagram represents solution resistance, and the constant phase element denotes the double layer capacitor.

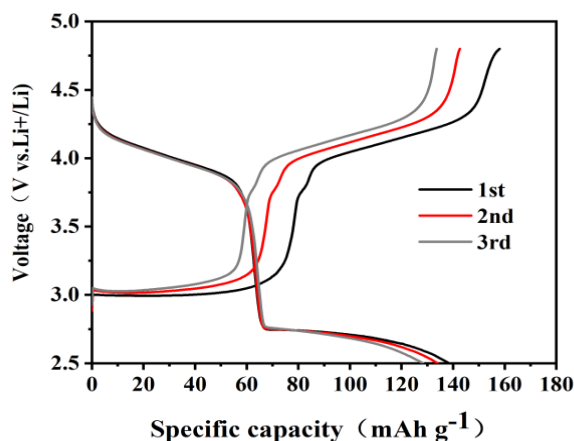


Fig. 5. Charge-discharge curves of  $\text{LiMn}_2\text{O}_4$  samples calcined at  $700\text{ }^\circ\text{C}$

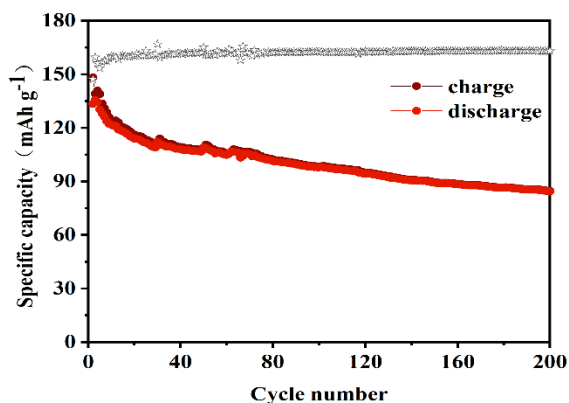


Fig. 6. Cycling performance of  $\text{LiMn}_2\text{O}_4$  samples at a calcination temperature of  $700\text{ }^\circ\text{C}$

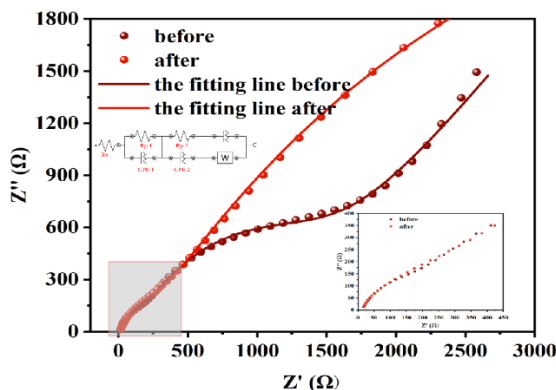


Fig. 7. Nyquist diagrams of  $\text{LiMn}_2\text{O}_4$  samples with calcination temperature of  $700\text{ }^\circ\text{C}$  and equivalent circuit diagrams

#### 4. CONCLUSION

High purity  $\text{LiMn}_2\text{O}_4$  material was successfully prepared using the high temperature solid phase method. This method is stable, controllable, and relatively simple. The structure and morphology of the material were characterized, revealing well-crystallized particles with irregular shapes and individual sizes ranging from 80 to 200 nm. In electrochemical tests, the  $\text{LiMn}_2\text{O}_4$  electrode, calcined at 700 °C, exhibited a first charging capacity of 158.0 mAh  $\text{g}^{-1}$  and a first discharging capacity of 138.4 mAh  $\text{g}^{-1}$ , demonstrating excellent electrochemical performance.

#### COMPETING INTERESTS

Authors have declared that no competing interests exist.

#### REFERENCES

1. Li M, Lu J, Chen Z, et al. 30 years of lithium-ion batteries [J]. *Advanced Materials*. 2018;30(33):1800561.
2. Wakihara M. Recent developments in lithium ion batteries [J]. *Materials Science and Engineering: R: Reports*. 2001;33(4): 109-134.
3. Kim T, Song W, Son D Y, et al. Lithium-ion batteries: Outlook on present, future, and hybridized technologies [J]. *Journal of Materials Chemistry A*. 2019;7(7): 2942-2964.
4. Scrosati B, Hassoun J, Sun YK. Lithium-ion batteries. A look into the future [J]. *Energy & Environmental Science*. 2011; 4(9):3287-3295.
5. Manthiram A. A reflection on lithium-ion battery cathode chemistry [J]. *Nature communications*, 2020;11(1):1550.
6. Xu B, Qian D, Wang Z, et al. Recent progress in cathode materials research for advanced lithium ion batteries [J]. *Materials Science and Engineering: R: Reports*. 2012;73(5-6):51-65.
7. Kim D K, Muralidharan P, Lee H W, et al. Spinel  $\text{LiMn}_2\text{O}_4$  nanorods as lithium ion battery cathodes [J]. *Nano Letters*. 2008; 8(11):3948-3952.
8. Zhao H, Nie Y, Li Y, et al. Low-cost and eco-friendly synthesis of octahedral  $\text{LiMn}_2\text{O}_4$  cathode material with excellent electrochemical performance [J]. *Ceramics International*. 2019;45(14):17183-17191.
9. Wu C, Xu M, Zhang C, et al. Cost-effective recycling of spent  $\text{LiMn}_2\text{O}_4$  cathode via a chemical lithiation strategy [J]. *Energy Storage Materials*. 2023;55:154-165.
10. Abou-Rjeily J, Bezza I, Laziz N A, et al. High-rate cyclability and stability of  $\text{LiMn}_2\text{O}_4$  cathode materials for lithium-ion batteries from low-cost natural  $\beta\text{-MnO}_2$  [J]. *Energy Storage Materials*. 2020;26: 423-432.
11. Hou X, Liu X, Wang H, et al. Specific countermeasures to intrinsic capacity decline issues and future direction of  $\text{LiMn}_2\text{O}_4$  cathode [J]. *Energy Storage Materials*. 2023;57:577-606.
12. Li L, Sui J, Qin W. Superior capacity, rate, long cycle life and high temperature performance of multilayered porous ultralong  $\text{LiMn}_2\text{O}_4$  nanorods for lithium ion batteries [J]. *Journal of Electroanalytical Chemistry*. 2019;833:304-312.
13. Nakayama M, Taki H, Nakamura T, et al. Combined computational and experimental study of Li exchange reaction at the surface of spinel  $\text{LiMn}_2\text{O}_4$  as a rechargeable Li-ion battery cathode [J]. *The Journal of Physical Chemistry C*. 2014; 118(47):27245-27251.
14. Xu W, He L, Zhao Z. Lithium extraction from high Mg/Li brine via electrochemical intercalation/de-intercalation system using  $\text{LiMn}_2\text{O}_4$  materials [J]. *Desalination*. 2021; 503:114935.
15. Li X, Xu Y, Wang C. Suppression of Jahn–Teller distortion of spinel  $\text{LiMn}_2\text{O}_4$  cathode [J]. *Journal of Alloys and Compounds*. 2009;479(1-2):310-313.
16. Chung K Y, Kim K B. Investigations into capacity fading as a result of a Jahn-Teller distortion in 4 V  $\text{LiMn}_2\text{O}_4$  thin film electrodes [J]. *Electrochimica Acta*. 2004; 49(20):3327-3337.
17. Xu W, Zheng Y, Cheng Y, et al. Understanding the effect of Al doping on the electrochemical performance improvement of the  $\text{LiMn}_2\text{O}_4$  cathode material [J]. *ACS Applied Materials & Interfaces*. 2021;13(38):45446-45454.
18. Capsoni D, Bini M, Chiodelli G, et al. Structural transition in Mg-doped  $\text{LiMn}_2\text{O}_4$ : A comparison with other M-doped Li–Mn spinels [J]. *Solid State Communications*. 2003;125(3-4):179-183.
19. Arumugam D, Kalaignan G P, Vediappan K, et al. Synthesis and electrochemical characterizations of nano-scaled Zn doped  $\text{LiMn}_2\text{O}_4$  cathode materials for rechargeable lithium batteries [J].

- Electrochimica Acta. 2010; 55(28): 8439-8444.
20. Shen C H, Liu R S, Gundakaram R, et al. Effect of Co doping in LiMn<sub>2</sub>O<sub>4</sub> [J]. Journal of Power Sources. 2001;102(1-2):21-28.
  21. Wei YJ, Yan LY, Wang CZ, et al. Effects of Ni doping on [MnO<sub>6</sub>] octahedron in LiMn<sub>2</sub>O<sub>4</sub>[J]. The Journal of Physical Chemistry B. 2004;108(48):18547-18551.
  22. Hou Y, Chang K, Tang H, et al. Drastic enhancement in the rate and cyclic behavior of LiMn<sub>2</sub>O<sub>4</sub> electrodes at elevated temperatures by phosphorus doping [J]. Electrochimica Acta. 2019;319: 587-595.
  23. Manjunatha H, Mahesh KC, Suresh GS, et al. The study of lithium ion de-insertion/insertion in LiMn<sub>2</sub>O<sub>4</sub> and determination of kinetic parameters in aqueous Li<sub>2</sub>SO<sub>4</sub> solution using electrochemical impedance spectroscopy [J]. Electrochimica Acta. 2011; 56(3): 1439-1446.
  24. Xu H, Cheng B, Wang Y, et al. Improved electrochemical performance of LiMn<sub>2</sub>O<sub>4</sub>/graphene composite as cathode material for lithium ion battery [J]. International Journal of Electrochemical Science. 2012;7(11):10627-10632.
  25. Kiani MA, Mousavi MF, Rahmanifar MS. Synthesis of nano-and micro-particles of LiMn<sub>2</sub>O<sub>4</sub>: Electrochemical investigation and assessment as a cathode in Li battery [J]. International Journal of Electrochemical Science. 2011;6(7):2581-2595.
  26. Huang J, Zhang J, Li Z, et al. Exploring differences between charge and discharge of LiMn<sub>2</sub>O<sub>4</sub>/Li half-cell with dynamic electrochemical impedance spectroscopy [J]. Electrochimica Acta. 2014;131:228-235.

© Copyright (2024): Author(s). The licensee is the journal publisher. This is an Open Access article distributed under the terms of the Creative Commons Attribution License (<http://creativecommons.org/licenses/by/4.0>), which permits unrestricted use, distribution, and reproduction in any medium, provided the original work is properly cited.

*Peer-review history:*  
*The peer review history for this paper can be accessed here:*  
<https://www.sdiarticle5.com/review-history/115430>